Optics Communications 387 (2017) 275–280

Contents lists available at ScienceDirect

Optics Communications

journal homepage: www.elsevier.com/locate/optcom

Comparison of multi-mode parallel detection microscopy methods

Dazhao Zhu[a], Yue Fang[a], Youhua Chen[a,c], Anwar Hussain[a,d], Cuifang Kuang[a,b,*], Zhihua Ding[a], Xu Liu[a,b]

[a] State Key Laboratory of Modern Optical Instrumentation, College of Optical Science and Engineering, Zhejiang University, Hangzhou 310027, China
[b] Collaborative Innovation Center of Extreme Optics, Shanxi University, Taiyuan 030006, China
[c] Key Laboratory of Instrumentation Science & Dynamic Measurement of Ministry of Education, North University of China, Taiyuan 030051, China
[d] Quantum Optics Lab, Department of Physic, COMSATS Institute of Information Technology Islamabad, Pakistan

ARTICLE INFO

Keywords:
Confocal microscopy
Fluorescence microscopy
Scanning
Microscopy

ABSTRACT

Four microscopy resolution enhancement methods based on parallel detection were investigated in this study: confocal microscopy with four pinhole sizes, fluorescence emission difference microscopy (FED) based on parallel detection, Airyscan microscopy, and virtual k-vector modulation optical microscopy (Vikmom). These methods use different algorithms to process parallel detection data and achieve resolution improvement. We investigated these methods first by performing simulations and then experimentally. In this report, the basic theories of these methods are briefly introduced. Then, analyses and comparisons of their imaging performances, especially in terms of resolution improvement, imaging speed, and signal-to-noise ratio, are presented. Finally, the results of our comparative study are summarized.

As a conventional microscopy method, confocal microscopy has been one of the most widely used tools in biotechnology and other fields. In principle, confocal microscopy can overcome the diffraction barrier by a factor of $\sqrt{2}$[1]; however, the theoretical resolution enhancement cannot be obtained practically because the pinhole cannot be infinitely small. In practice, as the pinhole becomes smaller, the detection efficiency deceases, resulting in reduction of the signal-to-noise ratio (SNR). Thus, the sample details still may not be resolvable in the final image even if the pinhole is sufficiently small and the setup is well adjusted. Although confocal microscopy cannot yield the desired resolution, many super-resolution methods based on the confocal system exist that can overcome the diffraction barrier; these include stimulated emission depletion (STED) microscopy [2] and fluorescence emission difference (FED) microscopy [3]. Furthermore, it is possible to enhance the resolution by employing an off-axis pinhole [4] or using the detection efficiency and resolution improvement method proposed by Sheppard [5], which have led to the development of super-resolution microscopy methods such as optical photon reassignment microscopy [6], image scanning microscopy [7], pixel reassignment microscopy [8], and Airyscan technology [9]. All of these methods and technologies are based on pinhole plane image detection and computational reassignment, with replacement of the single point detector that is used in a conventional confocal setup by a charge-coupled device (CCD), an avalanche diode array, or even a quadrant detector [10]. These detectors are employed to perform parallel detection, and then the data are processed using the corresponding algorithms to reconstruct high-resolution images.

In this paper, we discuss four microscopy methods based on the same parallel detection system: confocal microscopy with four pinhole sizes, parallel detection FED microscopy, Airyscan microscopy, and virtual k-vector modulation optical microscopy (Vikmom). One possible setup of the employed system is shown in Fig. 1. It is a simple conventional confocal microscopy system without a pinhole, but with the detector replaced by a parallel detector. The parallel detector is actually an array consisting of 61 single-point detectors arranged in a honeycomb pattern and numbered from 1 to 61, as shown in Fig. 1. Detector 1, which is in the center, has a diameter of 0.2 Airy units (AU); detectors 2–7 form the first ring of the honeycomb, which has a diameter of 0.6 AU; detectors 8–19 are in the second ring of the honeycomb, whose diameter is 1 AU; and detectors 20–37 form the second-to-last ring, which has a diameter of 1.25 AU.

The image of each detector in this arrangement is determined based on its position in the setup, as explained above. The center detector with a 0.2-AU-diameter pinhole generates a confocal image of the same size as the pinhole. In the single-detector confocal imaging setup, the off-axis pinholes are used to determine the off-axis geometry, while detector 1 provides the on-axis geometry. Therefore, 61 point spread function (PSFs), corresponding to the 61 detectors, are obtained. The PSF of each individual confocal system can be expressed as

* Corresponding author at: State Key Laboratory of Modern Optical Instrumentation, College of Optical Science and Engineering, Zhejiang University, Hangzhou 310027, China.
E-mail address: cfkuang@zju.edu.cn (C. Kuang).

http://dx.doi.org/10.1016/j.optcom.2016.11.067
Received 19 November 2016; Accepted 23 November 2016

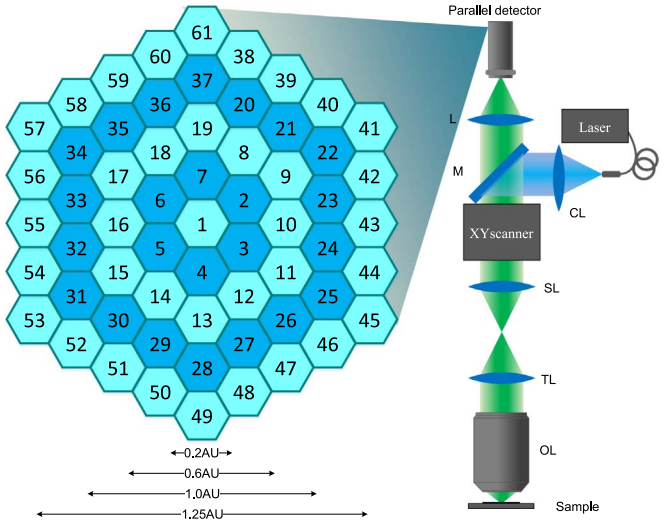

Fig. 1. System setup. CL, collimation lens; M, mirror; DM, dichromatic mirror; SL, scanning lens; TL, tube lens; OL, objective lens. The detectors are numbered from 1 to 61.

$$PSF_n = PSF_{exc} \times (PSF_{\mathrm{det}} \otimes P_n) \quad n = 1, 2, 3 \ldots, \tag{1}$$

where PSF_n is the nth confocal PSF, PSF_{det} is the corresponding detective PSF, PSF_{exc} is the system-exciting PSF, and P_n is the pinhole function.

The nth detector image I_n can be described by convolving the object function O_n with PSF_n and then replacing PSF_n with equation (1):

$$I_n = O_n \otimes [PSF_{exc} \times (PSF_{\mathrm{det}} \otimes P_n)] \quad n = 1, 2, 3 \ldots, \tag{2}$$

Since detective PSF is affected by the off-axis pinholes, the PSFs of the off-axis detectors have deformed shapes. The detector arrangement has central symmetry, therefore, each detector in the same ring has the same profile but a different shift direction. We present the PSFs of seven typical detectors (detectors 1, 4, 7, 13, 19, 28, and 37) to illustrate these features. The PSFs of these seven detectors, which were simulated using 488 nm exciting light and a numerical aperture of 1.51, are depicted in Fig. 2(a). As shown, the displacement of each PSF is proportional to the displacement of the corresponding detector. The larger the displacement is, the less energy is received. Consequently, the PSFs also become narrower and shorter with increasing displacement. We then normalized the PSFs of detectors 1, 4, 13, and 28 and shifted them back to the center, as shown in Fig. 2(b). The PSF of the detector farthest from the center (detector 28) is clearly the narrowest. Therefore, the detectors in the outer rings should theoretically generate images with resolutions higher than those of images obtained using detectors in the inner rings. Although their high-resolution signals may be overwhelmed by noise, the high-resolution information still can be used to retrieve clear images. In fact, each of the four methods discussed in this report can be used to extract this high-resolution information and restrain the effects of noise by processing the data from all of the detectors.

One merit of parallel detection is that confocal microscopy with different pinhole sizes can be performed relatively easily by taking information from detectors in different rings of the array. In this study, we performed confocal microscopy using 0.2-, 0.6-, 1.0-, and 1.25-AU-diameter pinholes. The confocal images $I_{confocal}$ obtained using differently sized pinholes can be described by

$$I_{confocal} = \sum_{m=1}^{n} I_m \quad n = 1, 2, 3 \ldots, \tag{3}$$

where m is the detector number and I_m is the image of the detector m. Therefore, the confocal image can be generated simply by summing the images of the individual detectors.

Next, FED imaging was conducted using the same setup. In traditional FED imaging, the final high-resolution image is obtained by performing a subtraction process, as is done in many microscopy methods [11]. A traditional FED image can be described using

$$I_{FED} = I_c - r \times I_n, \tag{4}$$

where I_c, In, and I_{FED} are the normalized intensity distributions of the confocal, negative confocal (doughnut spot scanning), and FED images, respectively, and r is the subtractive factor. Some negative intensity values will inevitably appear in the difference image after subtraction. The drawback of traditional FED microscopy is that two scans must be performed to obtain a single high-resolution image, which makes the setup relatively complicated and requires two exciting beams that are coaxially aligned with optical precision. However, these drawbacks do not exist when using parallel detection. In parallel detection, there is only one exciting beam and the setup can be adjusted easily. It is only necessary to obtain images from the detectors in a ring and in the center to replace the solid and doughnut spot exciting images, which is more convenient and allows for greater flexibility. In this investigation, we obtained images from relatively central detectors (detectors 1–7) and detectors in the outer rings (detectors 8–37) to generate an FED image, rewriting Eq. (4) as [12]

$$I_{FED} = \sum_{m=1}^{7} I_m - r \times \sum_{m=8}^{37} I_m, \tag{5}$$

Consequently, it was not necessary to shift the exciting light between solid and doughnut beams. We determined the optimal r value to be 0.55, to compute the results, which are shown in Fig. 4(f). The resolution is improved compared with that obtained using confocal microscopy. In a similar detection method called VAAS (Virtual Adaptable Aperture System) an additional detector, besides that used to capture the light that passes through the pinhole, is used to measure the light that does not pass through the pinhole [13,14]. In theory, parallel detection FED microscopy and VAAS should yield similar or even identical inner and outer PSFs. The main difference between these two methods is that the radii of the inner and outer rings can be chosen

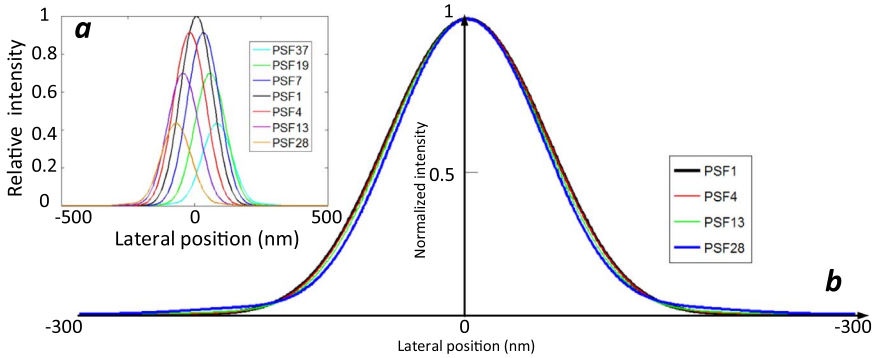

Fig. 2. (a) PSFs of detectors 1, 4, 7, 13, 19, 28, and 37; (b) normalized versions of PSFs from (a).